2016

Measurements of Thermodynamic Properties for R1123 and R1123+R32 Mixture

Yukihiro Higashi
Kyushu University, I2CNER, Japan, imufeehigashi@mac.com

Ryo Akasaka
Kyushu Sangyo University, Japan, ryo-a@ip.kyusan-u.ac.jp

Measurements of Thermodynamic Properties for R1123 and R1123+R32 Mixture

Yukihiro HIGASHI[1]*, Ryo AKASAKA[2]

[1]Kyushu University, Research Center for Next Generation Refrigerant Properties,
International Institute for Carbon-Neutral Energy Research(*I*^{2}*CNER*)
Nishi-ku, Fukuoka 810-0395, Japan
E-mail: imufeehigashi@mac.com

[2]Kyushu Sangyo University, Department of Mechanical Engineering
Higashi-ku, Fukuoka 813-8503, Japan
E-mail: ryo-a@ip.kyusan-u.ac.jp

* Corresponding Author

ABSTRACT

Measurements of $P\rho T$ and $P\rho Tx$ properties, vapor pressures, saturated densities and critical parameters were carried out for a new low GWP refrigerant R1123(trifluoroethylene; CF_2=CHF) and its binary mixture of R1123 + R32 system. Sixty-three $P\rho T$ property data and 13 vapor-pressure data for R1123 were obtained in the temperatures between 300 K and 430 K, pressures up to 6.9 MPa, and densities between 100 kg·m^{-3} and 900 kg·m^{-3} along 7 isochores. Twenty-one saturated densities for R1123 were obtained in the temperatures between 316.32 K and 331.73 K and densities between 222 kg·m^{-3} and 880 kg/m^3. On the basis of these measurements, the correlation of vapor pressures was proposed. Moreover, the critical parameters for R1123 were determined as T_c = 331.73 K, ρ_c = 504 kg·m^{-3}, and P_c = 4546 kPa. As for the binary R1123 + R32 mixture, the same kinds of measurements were carried out for the 40 mass% R1123 mixture and 60 mass% R1123 mixture. The composition dependence of the critical parameters for this mixture was also discussed.

1. INTRODUCTION

In order to solve the problems of ozone layer depletion as well as the global warming to be considered as important global environment problems, the searching for new alternatives of CFC(Chlorofluorocarbon), HCFC(Hydrochlorofluorocarbon), and HFC(Hydrofluorocarbon) refrigerants are very important task. Recently HFO(Hydrofluoroolefin) refrigerants such as R 1234yf (2,3,3,3-tetrafluoroprop-1-ene; $CF_3CF=CH_2$) and R 1234ze(E) (trans-1,3,3,3-tetrafluoroprop-1-ene; $CF_3CH=CHF$) have attracted considerable attention as a new low GWP refrigerant. Although these HFOs are very expected as the alternative refrigerants for the room air-conditioner and the heat pump system, there is the limit in the kind and the cost is too expensive. Therefore, it is very important to search for other new refrigerants as soon as possible.

As of now, R 32 is considered as the most prominent refrigerant of R22 or R410A alternatives in Japan because of its good thermodynamic properties and high system performance. Moreover, some of HFOs including R1234yf, R1234ze(E), and their mixtures are expected as another alternative refrigerant because of the feature of low GWP. New refrigerant R1123(trifluoroethylene; CF_2=CHF; Molar mass is 82.0245 g·mol^{-1}) has been appeared from Japanese refrigerant company (Tanaka *et al*., 2014). It is said thermophysical properties of this refrigerant is close to those of R32. However, the reliable information of thermodynamic properties for R1123 is insufficient. In the present study, thermodynamic properties of R1123 for $P\rho T$ (pressure-density-temperature) properties, vapor pressures, saturated vapor densities, saturated liquid densities, and critical parameters were measured. By analyzing the present results, the critical temperature T_c, critical density ρ_c, and critical pressure P_c for not only R1123 but also its mixture was determined by the direct observation of meniscus disappearance. The vapor pressure correlation is also proposed. Moreover, thermodynamic properties for the R1123 + R32 mixtures are reported.

2. EXPERIMENTAL APPARATUS

2.1 Measurements of $P\rho Tx$ Properties and Vapor Pressures

Schematic diagram of the experimental apparatus to measure $P\rho Tx$ properties and vapor pressures for R1123 as well as those for R1123 + R32 mixture is shown in Figure 1. The experimental apparatus and procedures were described in our previous papers (Kobayashi *et al*., 2011; Higashi *et al.*, 2015). Pressure vessel[A] made of stainless steel was installed in a silicon-oil thermostated bath. Temperature of silicone-oil in the bath was kept constant within 5 mK using PID controller[F], main heater[I], sub heater[J], and stirrer[K]. The cooler[L] was not used in this experiment. Temperature was measured with a 25 Ω standard platinum resistance thermometer[D] (Chino, model R800-2) calibrated against ITS-90 with an aid of AC thermometer bridge[E] (Tinsley, model 5840). The uncertainty of the temperature measurements was estimated within 10 mK taking into consideration temperature fluctuation in the bath and the accuracy of thermometer. Pressure was measured with the pressure sensor[B] (Paroscientifics, Model 42K-101) connected to the pressure vessel directly. The uncertainty of pressure measurements was estimated within 2 kPa. The density was determined from the sample mass and the inner volume of pressure vessel with tubing and valves. The mass of sample was measured with a precision balance (Mettler Toledo, Model XP1203S) with the uncertainty of ±1 mg. The inner volume of the pressure vessel including the tubing and valves was measured by using the reference fluids in the wide temperature and pressure ranges. In the present experiment, R32 and R134a were used as reference fluids to determine the inner volumes. The uncertainty of the density measurements was estimated within 0.05 %. The uncertainty of the composition measurements is estimated to be within ±0.05%.

The high-grade samples of R1123 and R32 were directly supplied from Asahi Glass Co., Japan. The sample purities of R1123 and R32 reported by the supplier are 99.9 mol% and 99.5 mol%, respectively.

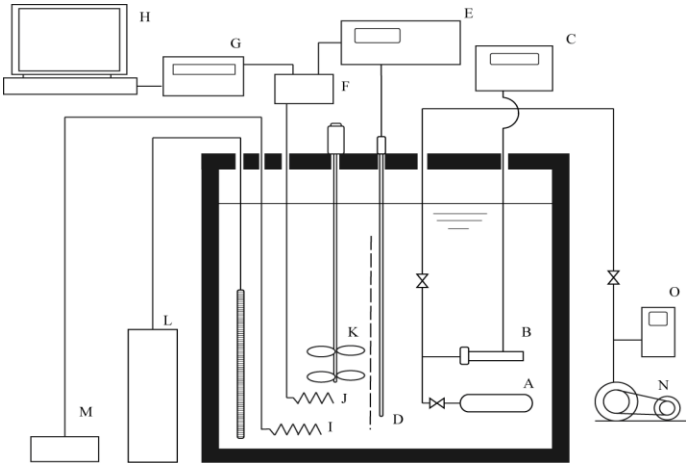

A: sample vessel, B: pressure sensor,
C: pressure indicator,
D: 25Ω platinum resistance thermometer,
E: thermometer bridge, F: PID controller,
G: digital multimeter, H: computer,
I: main heater, J: sub heater, K: stirrer,
L: cooler, M: voltage transformer,
N: vacuum pump, O: vacuum indicator

Figure 1: Experimental apparatus for $P\rho Tx$ property measurements.

2.2 Measurements of Vapor-Liquid Coexistence Curve and Critical Parameters

The experimental apparatus for measuring the saturated liquid and vapor densities is shown in Figure 2. The experimental apparatus and procedures were described in our previous papers (Okazaki *et al*., 1983; Higashi, 1994). The main portion of the apparatus is composed of three high-pressure vessels. The optical cell[C] with two Pyrex glass windows was used for observing the meniscus disappearance of the sample. This optical cell was a SUS-304 barrel-type cylindrical vessel and its inner volume is 11.638 ± 0.008 cm^3, which was calibrated by filling pure water at room temperature condition. The expansion vessel [B] and supplying vessel [A] were used to change the sample density in the optical cell without new sample charge. The inner volumes of the expansion vessel and supplying vessel are 8.949 ± 0.003 cm^3 and 77.575 ± 0.016 cm^3, respectively. The experimental apparatus was installed in a silicone-oil bath. The temperature fluctuation in the oil bath was controlled within 5 mK using 1.5 kW heater[M] and 300 W heater[L], with an aid of PID control system [F, G]. The temperature measurement was conducted with 25Ω standard platinum resistance thermometer[I] (Chino: RF800-2) calibrated against ITS-90 and AC thermometer bridge[D1] (ASL: F700). The uncertainty of temperature measurement depends upon the precision of the thermometer used and the temperature fluctuation in the oil bath. In this experiment, the uncertainty of temperature measurements was estimated to be within 10 mK. The sample density in the optical cell can be calculated from the mass of the sample and the inner volumes of

three pressure vessels for each expansion procedure. The uncertainty of density measurements is corresponding to the times of expansion. In this experiment, the uncertainty of density measurements is estimated to be within 0.06 % to 0.25 %. The uncertainty of the composition measurements is estimated to be within 0.05%.
The samples of R1123 and R32 used in this measurement were supplied from Asahi Glass Co., Japan. The sample purities of R1123 and R32 are 99.9 mol% and 99.5 mol%, respectively.

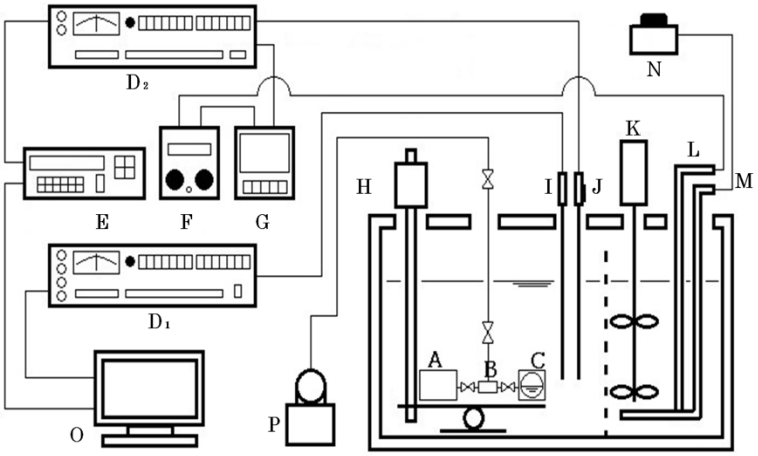

A: supplying vessel, B: expansion vessel,
C: optical cell, D_1, D_2: thermometer bridge,
E: digital multimeter, F: voltage converter,
G: PID controller, H: rocking stage,
I, J: 25Ω platinum resistance thermometer,
K: stirrer, L: 300W heater,
M: 1.5 W heater, N: voltage transformer,
O: Computer.

Figure 2: Experimental apparatus for measuring saturated densities.

3. THERMODYNAIC PROPERTIES FOR R1123

3.1 *PρT* Properties and Vapor Pressures

Sixty-three *PρT* property data for R1123 were obtained in the temperature range from 300 K to 430 K, in the density range between 100 kg·m^{-3} and 900 kg·m^{-3}, and in the pressure range up to 6.9 MPa. In the two-phase region, *PρT* property data correspond to vapor pressure data. Thirteen vapor-pressure data were obtained in the temperature range between 300 K and 330 K. The numerical data of vapor pressures and *PρT* properties are summarized in Tables 1 and 2, respectively. Experimental results along seven isochores are shown in Figure 3 on pressure-temperature diagram. Vapor-pressure data for R1123 together with vapor-pressure curves for R32, R134a, R1234yf and R410A calculated by REFPROP 9.1(Lemmon et al., 2013) are drawn in Figure 4 on pressure-temperature plane. It is found that the vapor pressure curve for R1123 shown in Figure 4 is close to that for R32. In Table 1, the vapor-pressure data measured at the temperature of 331.73 K is considered as the critical pressure determined by the experiment directly, because the temperature of 331.73 K is determined as the critical temperature.

Table 1: Vapor pressure data of R1123

T (K)	P_s (kPa)	T (K)	P_s (kPa)	T (K)	P_s (kPa)
300.00	2222.1	313.00	3015.4	325.00	3931.3
303.00	2388.2	315.00	3155.0	328.00	4194.2
305.00	2504.7	318.00	3373.3	330.00	4377.7
308.00	2687.8	320.00	3525.7	331.73*	4543.4*
310.00	2815.3	323.00	3764.5		

(*) This data was obtained at the critical temperature.

Table 2: $P\rho T$ property data for R1123

T (K)	P (kPa)	ρ (kg m^{-3})	T (K)	P (kPa)	ρ (kg m^{-3})	T (K)	P (kPa)	ρ (kg m^{-3})
310.00	2252.2	99.8	380.00	5363.2	199.6	338.00	5730.4	699.5
320.00	2390.1	99.7	390.00	5656.0	199.6	340.00	6065.8	699.4
330.00	2524.7	99.6	400.00	5945.9	199.4	342.00	6404.3	699.4
340.00	2656.7	99.5	410.00	6232.2	199.3	344.00	6745.4	699.3
350.00	2786.6	99.5	420.00	6515.8	199.1	326.00	4315.3	799.8
360.00	2914.8	99.4	335.00	4587.9	300.2	328.00	4753.1	799.7
370.00	3041.4	99.4	340.00	4861.0	300.1	330.00	5196.0	799.6
380.00	3166.7	99.4	350.00	5393.2	300.0	332.00	5643.1	799.5
390.00	3290.7	99.3	360.00	5912.1	299.9	334.00	6094.5	799.4
400.00	3414.1	99.3	370.00	6421.9	299.8	336.00	6548.9	799.3
410.00	3536.2	99.2	333.00	4667.9	499.8	316.00	3655.7	899.6
420.00	3657.4	99.1	335.00	4864.3	499.8	317.00	3956.7	899.5
430.00	3777.5	99.0	340.00	5359.2	499.6	318.00	4258.0	899.4
320.00	3481.7	200.2	345.00	5856.8	499.5	319.00	4560.8	899.3
323.00	3585.1	200.1	350.00	6356.5	499.4	320.00	4864.3	899.2
325.00	3653.0	200.1	355.00	6857.8	499.3	321.00	5168.8	899.1
330.00	3819.8	200.0	330.00	4432.1	699.9	322.00	5474.4	899.0
340.00	4143.5	199.9	331.00	4588.8	699.8	323.00	5780.8	899.0
350.00	4457.6	199.8	332.00	4747.3	699.8	324.00	6088.1	898.9
360.00	4764.8	199.7	334.00	5070.3	699.7	325.00	6396.1	898.8
370.00	5066.3	199.7	336.00	5398.1	699.6	326.00	6704.6	898.7

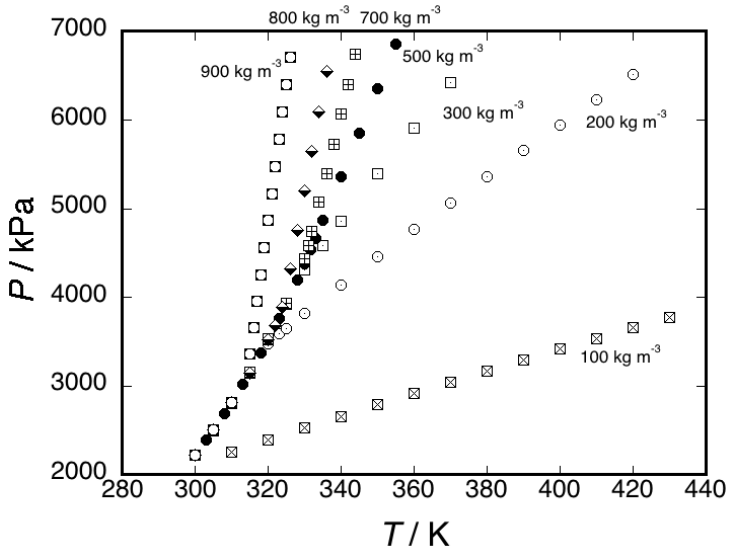

Figure 3: $P\rho T$ property data for R1123.

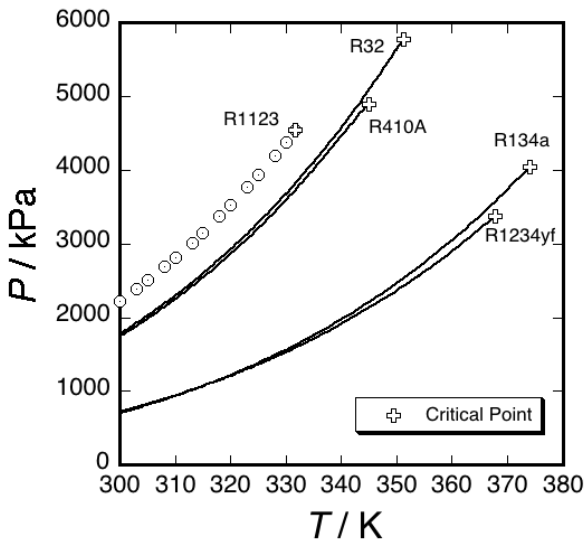

Figure 4: Vapor pressure data for R1123.

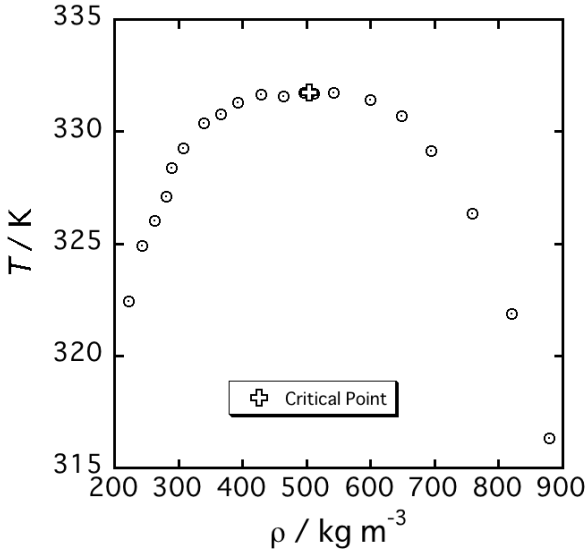

Figure 5: Saturated vapor and liquid densities in the critical region for R1123.

Table 3: Saturated liquid and saturated vapor densities data for R1123.

T (K)	ρ (kg·m^{-3})	T (K)	ρ (kg·m^{-3})	T (K)	ρ (kg·m^{-3})
322.412	222.1	330.794	366.3	331.728*	542.8*
324.912	242.6	331.289	392.7	331.428	599.6
326.010	262.1	331.645	429.0	330.692	648.0
327.096	280.9	331.591*	463.5*	329.135	694.6
328.399	289.5	331.727*	496.8*	326.358	758.9
329.272	306.9	331.725*	505.2*	321.854	820.3
330.395	339.0	331.717*	512.1*	316.324	879.5

(*) Critical opalescence were observed.

3.2 Saturated Vapor and Liquid Densities near the Critical Point

The saturated vapor and saturated liquid densities for R1123 were determined by the visual observation of meniscus disappearance. Twelve saturated vapor density data, eight saturated liquid density data, and one data which is the closest data to critical density, were obtained in the temperature range between 316.32 K and 331.73 K, and in the density range from 222 kg·m^{-3} to 880 kg·m^{-3}. Vapor-liquid coexistence curve near the critical point for R1123 are drawn in Figure 5 on temperature-density plane, and the numerical data are summarized in Table 3.

3.3 Determination of the Critical Temperature and Critical Density for R1123

On the basis of the meniscus observation in the critical region, the critical temperature and critical density of R1123 were determined in consideration of the meniscus disappearing level as well as the intensity of critical opalescence. The critical opalescence was observed at five densities from 463.5 kg·m^{-3} to 542.8 kg·m^{-3} marked with an asterisk in Table 3. The meniscus at the density of 463.5 kg·m^{-3} and 496.8 kg·m^{-3} was located at the center level in the optical cell at room temperature. With increasing temperature, the meniscus level gradually descended but disappeared prior to reaching the bottom of the optical cell. This is the meniscus behavior of saturated vapor. The meniscus at the density of 512.1 kg·m^{-3} and 542.8 kg·m^{-3} was located at the center level in the optical cell at the room temperature. With increasing temperature, the meniscus level gradually ascended but disappeared prior to reaching the top of the optical cell. This is the meniscus behavior of saturated liquid. The meniscus at the density of 505.2 kg·m^{-3} was located

at the center level in the optical cell at the room temperature. This meniscus level was unchanged at the center in the optical cell with increasing temperature and finally disappeared at that level. The intensity of the critical opalescence in the vapor phase was almost the same as the liquid phase. This density is considered to be close to the critical density, Finally, the critical parameters for R1123 were experimentally determined as follows: T_c = 331.73 ± 0.01 K and ρ_c = 504 ± 3 kg·m^{-3}.

3.4 Vapor Pressure Correlation and Critical Pressure

By using the present vapor-pressure data, vapor pressure correlations for R1123 were formulated. The functional form of the vapor pressure correlation is the same as that for R 1234yf (Tanaka and Higashi, 2010a), R 1234ze(E) (Tanaka *et al*. 2010a), and R1234ze(Z) (Higashi *et al*. 2015).

$$\ln P = \ln P_c + (T_c / T)(A\tau + B\tau^{1.5} + C\tau^{2.5} + D\tau^5), \quad (1)$$

where $\tau = 1-T/T_c$. The T_c values determined in the present work were adopted in Eq. (1). Coefficients of *A* through *D* and the critical pressure P_c are treated as fitting parameters. The critical temperature, critical pressure, and coefficients *A* through *D* for R1123 are summarized in Table 4. The critical pressure for R1123 was determined as P_c = 4546 ± 3 kPa.

Table 4: Coefficients of vapor pressure correlation of Eq. (1)

T_c / K	P_c / kPa	*A*	*B*	*C*	*D*
331.73	4546.1	-7.36327	2.42255	-5.26879	-4.00891

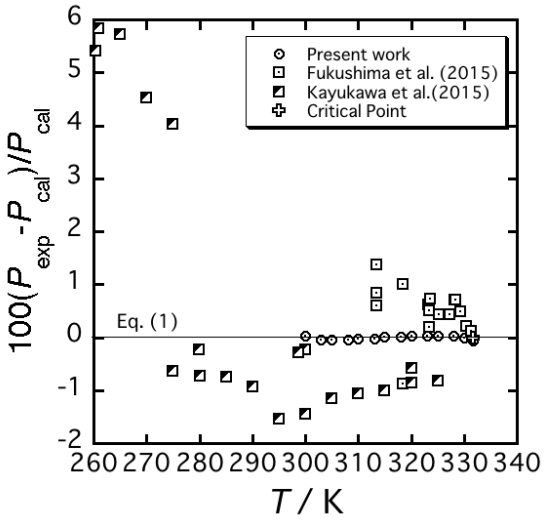

Figure 6: Deviation plots of vapor pressures for R1123 against the present correlation, Eq. (1).

The absolute deviations of vapor pressures between the experimental data and the calculation values by Eq. (1) are shown in Figure 6. Equation (1) reproduces the present vapor pressure data as the average deviation within 0.03 %. Fukushima *et al.*(2015) and Kayukawa *et al*.(2015) had already measured the vapor pressures for R1123. Fukushima *et al.* measured the vapor pressures for R1123 in the temperatures between 313 and 331 K. All of their data exist in the high temperature region and have larger deviations against Eq. (1). Kayukawa *et al.* had measured in the wide temperature range including the very low temperature region. Vapor pressure data by Kayukawa *et al.* in the low temperatures have large scatters against Eq. (1).

With respect to the critical parameters for R1123, Fukushima *et al.* (2015) have measured with the meniscus observation. Their reported critical parameters for R1123 are T_c = 331.80 ± 0.05 K, ρ_c = 510 ± 5 kg·m^{-3}, and P_c = 4545 ± 5 kPa. Most of critical parameters are in good agreement with the present work.

4. THERMODYNAIC PROPERTIES FOR R1123 + R32 MIXTURE

4.1 *PρTx* Properties

Fifty *PρTx*-property data for 60.00 mass% R1123 + 40.00 mass% R32 mixture were obtained along six isochores in the densities from 100 kg·m^{-3} to 900 kg·m^{-3}. Whereas fifty-one *PρTx*-property data for 40.00 mass% R1123 + 60.00 mass% R32 mixture were obtained along six isochores in the densities from 100 kg·m^{-3} to 900 kg·m^{-3}. *PρTx*-property data distribution are drawn in Figures 7 and 8 for 60 mass% R1123 and 40 mass% R1123, respectively. The numerical data of *PρTx* properties are also summarized in Tables 5 and 6.

Table 5: *PρTx* property data for 40.00 mass% R1123 + 60.00 mass% R32 (One-phase region)

T (K)	*P* (kPa)	*ρ* (kg m^{-3})	*T* (K)	*P* (kPa)	*ρ* (kg m^{-3})	*T* (K)	*P* (kPa)	*ρ* (kg m-3)
313.00	2740.6	99.0	350.00	5183.9	199.8	337.00	4903.8	699.9
315.00	2782.0	99.0	360.00	5626.8	199.7	338.00	5123.0	699.9
318.00	2843.2	98.9	370.00	6059.0	199.7	339.00	5343.9	699.9
320.00	2883.7	98.9	380.00	6482.8	199.6	340.00	5567.3	699.8
330.00	3081.4	98.8	341.00	5212.2	300.0	341.00	5792.5	699.8
340.00	3273.0	98.8	343.00	5367.7	300.0	342.00	6019.0	699.7
350.00	3459.9	98.7	345.00	5521.0	300.0	343.00	6247.2	699.7
360.00	3643.0	98.7	350.00	5895.4	299.9	344.00	6476.3	699.7
370.00	3822.8	98.7	355.00	6262.7	299.9	345.00	6706.7	699.7
380.00	4000.1	98.6	360.00	6625.2	299.8	316.00	3760.8	900.1
390.00	4174.5	98.6	342.21	5384.0	452.9	317.00	4190.7	899.9
400.00	4347.3	98.5	344.00	5590.7	452.8	318.00	4623.6	899.8
410.00	4517.7	98.5	346.00	5822.2	452.8	319.00	5055.1	899.8
420.00	4686.5	98.3	348.00	6053.8	452.8	320.00	5487.4	899.7
430.00	4853.5	98.2	350.00	6286.4	452.7	321.00	5920.5	899.6
335.00	4488.7	199.9	352.00	6519.8	452.7	322.00	6354.8	899.5
340.00	4726.1	199.9				323.00	6790.0	899.4

Table 6: *PρTx* property data for 60.00 mass% R1123 + 40.00 mass% R32

T (K)	*P* (kPa)	*ρ* (kg m^{-3})	*T* (K)	*P* (kPa)	*ρ* (kg m^{-3})	*T* (K)	*P* (kPa)	*ρ* (kg m^{-3})
310.00	2589.4	99.9	360.00	5430.4	199.6	350.00	6493.7	469.7
315.00	2681.6	99.9	370.00	5817.2	199.6	352.00	6719.8	469.7
320.00	2772.0	99.8	380.00	6197.0	199.5	336.00	5038.5	674.1
330.00	2948.5	99.7	390.00	6570.8	199.4	337.00	5221.9	674.1
340.00	3120.3	99.7	338.00	5055.5	300.1	338.00	5407.6	674.0
350.00	3288.5	99.6	340.00	5196.1	300.1	340.00	5783.7	674.0
360.00	3453.5	99.6	350.00	5876.3	300.0	342.00	6165.6	673.9
370.00	3616.0	99.6	360.00	6535.3	299.9	344.00	6552.4	673.8

Table 6: *PρTx* property data for 60.00 mass% R1123 + 40.00 mass% R32 (continued)

T (K)	*P* (kPa)	*ρ* (kg m^{-3})	*T* (K)	*P* (kPa)	*ρ* (kg m^{-3})	*T* (K)	*P* (kPa)	*ρ* (kg m^{-3})
380.00	3776.3	99.5	345.00	5539.6	300.0	315.00	3492.8	900.0
390.00	3934.5	99.5	355.00	6207.5	299.9	316.00	3877.3	899.9
400.00	4091.3	99.5	338.01	5152.1	470.0	317.00	4261.9	899.8
410.00	4246.2	99.4	339.00	5261.8	470.0	318.00	4648.4	899.7
420.00	4399.8	99.3	340.00	5372.9	469.9	319.00	5036.2	899.6
430.00	4551.9	99.1	342.00	5595.4	469.9	320.00	5424.2	899.5
330.00	4204.2	199.9	344.00	5818.9	469.8	321.00	5813.3	899.4
340.00	4628.0	199.8	346.00	6043.1	469.8	322.00	6203.6	899.3
350.00	5034.9	199.7	348.00	6268.0	469.8	323.00	6594.8	899.3

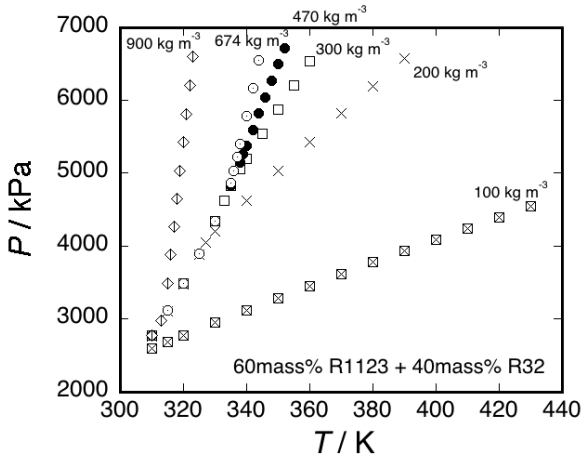

Figure 7: *PρTx* property data for 60 mass% R1123 + 40 mass% R32.

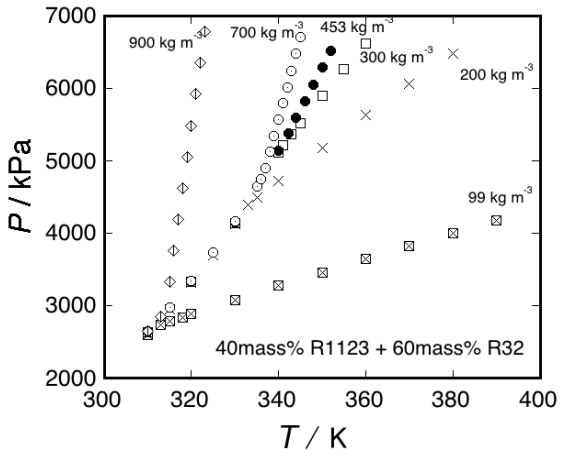

Figure 8: *PρTx* property data for 40 mass% R1123 + 60 mass% R32.

4.2 Vapor-Liquid Coexistence Curve near the Critical Point

Similar with pure R1123, the saturated vapor and liquid densities for the R1123 + R32 mixture near the critical point were determined by the visual observation of meniscus disappearance. The saturated densities for the R1123 + R32 mixture are summarized in Tables 7 and 8, and coexistence curves are drawn in Figure 9.

Table 7: Saturated liquid and saturated vapor densities data for R1123.
(a) 59.9 mass% R1123 and 40.1 mass% R32 mixture

T (K)	*ρ* (kg·m^{-3})	*T* (K)	*ρ* (kg·m^{-3})	*T* (K)	*ρ* (kg·m^{-3})	*T* (K)	*ρ* (kg·m^{-3})
326.840	193.9	335.434	294.3	338.013*	473.5*	335.187	658.8
328.870	210.6	336.459	317.4	338.012*	479.4*	332.777	710.7
331.820	245.4	336.977	342.9	337.971*	520.6*	328.758	767.9
333.363	266.4	337.521	372.4	337.716*	561.5*	322.336	834.1
333.863	271.0	338.033	401.6	336.737	606.6		

Table 8: Saturated liquid and saturated vapor densities data for R1123. (continued)
(b) 40.1 mass% R1123 and 59.9 mass% R32 mixture

T (K)	ρ (kg·m^{-3})	T (K)	ρ (kg·m^{-3})	T (K)	ρ (kg·m^{-3})	T (K)	ρ (kg·m^{-3})
333.790	205.9	342.165	364.2	342.145*	467.2*	338.920	644.3
335.536	226.8	342.121	401.1	342.093*	509.1*	335.671	709.8
338.199	250.6	342.265	422.9	341.574	560.8	332.714	748.4
340.409	287.8	342.267*	443.2*	340.943	591.3	325.812	815.7
341.090	317.0						

(*) Critical opalescence were observed.

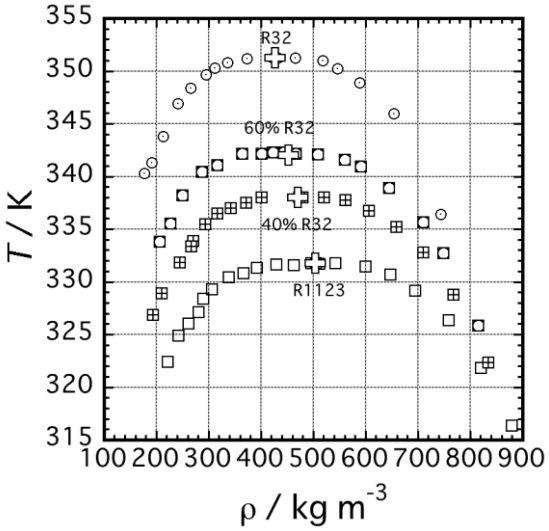

Figure 9: Saturated vapor and liquid densities for the R1123+R32 mixture.

Table 9: Critical parameters for the R1123 + R32 mixture.

w_{32}	x_{32}	T_c / K	P_c / kPa	ρ_c / kg m^{-3}	V_c / cm^3 mol^{-1}
1 (= R32)	1 (= R32)	351.26 ± 0.01	5785 ± 9	427 ± 5	121.8 ± 1.5
0.599	0.702	342.21 ± 0.03	5384 ± 3	453± 5	134.5 ± 1.5
0.401	0.514	338.01 ± 0.02	5152 ± 5	470 ± 3	141.8 ± 0.9
0 (= R1123)	0 (= R1123)	331.73 ± 0.01	4546 ± 3	504 ± 3	162.7 ± 0.9

The critical parameters of the R1123 + R32 mixture were determined by the same procedure for pure R1123 in Section 3.3. The critical points determined in the present work are plotted in Figure 9 with cross symbol. And numerical values of the critical parameters for the R1123 + R32 are summarized in Table 9.

4.3 Composition Dependence of the Critical Parameters (Critical Locus)

On the basis of the critical parameters determined in the previous section, the correlation of critical locus for the R1123 + R32 mixture was formulated. As for the functional form of the critical locus correlation, the following equations (Higashi et al., 1988) was adopted.

$$T_{cm} = q_1 T_{c1} + q_2 T_{c2} + 2 q_1 q_2 \Delta_T \quad (2)$$

$$V_{cm} = q_1 V_{c1} + q_2 V_{c2} + 2 q_1 q_2 \Delta_V \quad (3)$$

$$P_{cm} = q_1 P_{c1} + q_2 P_{c2} + 2 q_1 q_2 \Delta_P \quad (4)$$

$$r_{cm} = 1000 M_m / V_{cm} \quad (5)$$

$$q_i = x_i V_{ci}^{2/3} / \sum_j x_j V_{cj}^{2/3} \quad (6)$$

In Eqs. (2) to (4), T_{cm} in K, V_{cm} in cm^3 mol^{-1}, P_{cm} in kPa, and ρ_{cm} in kg m^{-3} denote the critical temperature of mixture, the critical molar volume of mixture, the critical pressure of mixture and the critical density of mixture, respectively. M_m in g mol^{-1} denotes the molar mass of mixture. Subscript 1 and 2 denote the properties of R1123 and R32, respectively. The molar mass of the R1123 and R32 are 82.0245 g mol^{-1} and 52. 0234 g mol^{-1}, respectively. When the critical parameters for pure R1123 and pure R32 in Table 9 were used, the adjustable parameter of Δ_T , Δ_V and Δ_P in Eqs. (2) to (4) must be Δ_T = -5.5 K, Δ_V = -3.7 cm^3 mol^{-1}, and Δ_P = 51 kPa, respectively.

5. CONCLUSIONS

Pρ*T* and *P*ρ*Tx* properties, vapor pressures, and saturated densities for R1123 and R1123+R32 mixture were measured. On the basis of these measurements, the correlation of vapor pressures was also proposed. The critical parameters for R1123 were determined as T_c = 331.73 K, ρ_c = 504 kg/m^3, and P_c = 4546 kPa. Moreover, the composition dependence of the critical parameters for the R1123 + R 32 mixture was also determined.

REFERENCES

Fukushima, M., Hayamizu, H., & Hashimoto, M.,(2015). Thermodynamic properties of low-GWP alternative refrigerants. *Proc. 24th IIR International Congress of Refrigeration*, Yokohama, Japan.

Higashi, Y., Kabata, Y., Uematsu, M., & Watanabe, K. (1988). Measurements of the vapor-liquid coexistence curve for the R13B1 + R114 system in the critical region. *J. Chem. Eng. Data*, 33(1), 23-26.

Higashi, Y. (1994). Critical parameters for HFC134a, HFC32 and HFC125. *Int. J. Refrig.*, 17(8), 524-531.

Higashi, Y., Hayasaka, S., Shirai, C., & Akasaka, R. (2015). Measurements of *P*ρ*T* properties, vapor pressures, saturated densities and critical parameters for R 1234ze(Z) and R 245fa. *Int. J. Refrig.*, 52, 100-108.

Kayukawa, Y., Kano, Y., Fujita, Y., Hashimoto, M., & Fukushima, M. (2015), Measurements for vapor pressures and *PVT* properties for low-GWP refrigerant, HFO-1123, by a magnetic levitation densimeter. *JSRAE 2015 Annual Conference*, Tokyo, Japan.

Kobayashi, K., Tanaka, K., & Higashi, Y. (2011). *P*ρ*Tx* property measurements of binary HFO-1234ze(E) + HFC-32 refrigerant mixtures. *Trans. of the JSRAE*, 28(4): 415-426 (in Japanese).

Lemmon, E. W., Huber, M. L., & McLinden, M. O. (2013). NIST Standard Reference Database 23: Reference Fluid Thermodynamic and Transport Properties – REFPROP Version 9.1, NIST, USA.

Okazaki, S., Higashi, Y., Takaishi, Y., Uematsu, M., & Watanabe, K. (1983). Procedures for determining the critical parameters of fluids, *Rev. Sci. Instrum.*, 54(1), 21-25.

Tanaka, K. & Higashi, Y. (2010). Thermodynamic properties of HFO-1234yf(2,3,3,3-tetrafluoropropene). *Int. J. Refrig.*, 33(3), 474-479.

Tanaka, K., Takahashi, G., & Higashi, Y. (2010). Measurements of the vapor pressures and *P*ρ*T* properties for trans-1,3,3,3- tetrafluoropropene (HFO-1234ze(E)). *J. Chem. Eng. Data.*, 55(6), 2169-2172.

Tanaka, T., Okamoto, H., Ueno, K., Irisawa, J., Otsuka, T., Noigami, T., & Dobashi, R. (2014). Development of a new low-GWP refrigerant composed of HFO-1123(trifluoroethylene). AIChE Annual Meeting,

ACKNOWLEDGEMENT

The author is grateful to Asahi Glass Co., Japan, for furnishing the high-grade sample of R1123 and R 32. The author thanks to Mr. Chihiro Shirai, who is my student of Iwaki Meisei University, for his valuable assistance in carrying out the experiment.